Biochimica et Biophysica Acta 1818 (2012) 1274–1283

Contents lists available at SciVerse ScienceDirect

Biochimica et Biophysica Acta

journal homepage: www.elsevier.com/locate/bbamem

Charge distribution and imperfect amphipathicity affect pore formation by antimicrobial peptides

Maja Mihajlovic, Themis Lazaridis *

Department of Chemistry, The City College of New York, 160 Convent Ave, New York, NY 10031, USA

ARTICLE INFO

Article history:
Received 24 August 2011
Received in revised form 14 January 2012
Accepted 17 January 2012
Available online 25 January 2012

Keywords:
Molecular dynamics simulation
Antimicrobial peptide
Charge distribution
Imperfect amphipathicity
Melittin
Magainin MG-H2

ABSTRACT

Antimicrobial peptides often permeabilize biological membranes via a pore mechanism. Two pore types have been proposed: toroidal, where the pore is partly lined by lipid, and barrel-stave, where a cylindrical pore is completely lined by peptides. What drives the preference of antimicrobial peptides for a certain pore type is not yet fully understood. According to neutron scattering and oriented circular dichroism, melittin and MG-H2 induce toroidal pores whereas alamethicin forms barrel-stave pores. In previous work we found that indeed melittin seems to favor toroidal pores whereas alamethicin favors cylindrical pores. Here we designed mutants of these two peptides and the magainin analog MG-H2, aimed to probe how the distribution of charges along the helix and its imperfectly amphipathic structure influence pore formation. Molecular dynamics (MD) simulations of the peptides in a pre-formed cylindrical pore have been performed. The duration of the simulations was 136 ns to 216 ns. We found that a melittin mutant with lysine 7 neutralized favors cylindrical pores whereas a MG-H2 mutant with lysines in the N-terminal half of these peptides neutralized and an alamethicin mutant with a positive charge at the position 7 form semitoroidal pores. These results suggest that charged residues within the N-terminal half are important for toroidal pore formation. Toroidal pores produced by MG-H2 are more disordered than the melittin pores, likely because of the charged residues located in the middle of the MG-H2 helix (K11 and K14). Imperfect amphipathicity of melittin seems to play a role in its preference for toroidal pores since the substitutions of charged residues located within the nonpolar face by hydrophobic residues suppress evolution of a toroidal pore. The mutations change the position of lysine 7 near the N-terminus, relative to the lower leaflet headgroups. The MD simulations also show that the melittin P14A mutant forms a toroidal pore, but its configuration diverges from that of melittin and it is probably metastable.

1. Introduction

Antimicrobial peptides (AMPs) are found in all organisms, from invertebrates and plants to humans, as components of the innate immune system [1,2]. They are active against bacteria, fungi, parasites, enveloped viruses and cancer cells [2–8]. Recently, AMPs have been found to play a role in cardiovascular pathophysiology as well [9]. Since AMPs target cell membranes directly and bacteria are less likely to develop resistance to them, they have potential as antibiotic agents [10]. However, the origin of their cell selectivity and their mechanism of action are still not well understood. Cell selectivity is usually attributed to differences between prokaryotic and eukaryotic membranes. Prokaryotic membranes, which contain anionic lipids, are often targeted by cationic antimicrobial peptides, although other factors besides electrostatics seem to play a role [6,11,12].

AMPs are usually unstructured in solvent but fold into amphiphilic α-helices in the presence of membranes. Less often they form β-sheets or remain unfolded. Depending on the peptide-to-lipid ratio, AMPs bind to the membrane surface or, at higher ratios, insert into them forming pores that depolarize the membrane, thus killing the cell (the pore mechanism) [13]. Alternatively, they can induce membrane disintegration and/or micellization (the carpet mechanism) [14]. Two types of pores have been proposed: barrel-stave (cylindrical) pores and toroidal pores. In the classical view, the barrel-stave pore is a highly ordered structure in which a cylindrical water pore is lined by peptides in transmembrane orientation and in direct contact with each other [15,16]. In the toroidal pore, the membrane bends so that headgroups from the lower and upper leaflet connect. A central water pore is thus lined both by peptides and lipid headgroups. It is thought that the pore is highly ordered, with its radius smallest in the middle of the bilayer and largest at the ends [17–20].

Abbreviations: MD, molecular dynamics; AMT, alamethicin; MLT, melittin; AMP, antimicrobial peptide; DMPC, 1,2-dimyristoyl-*sn*-glycero-3-phosphocholine; DPPC, 1,2-dipalmitoyl-*sn*-glycero-3-phosphocholine; POPC, 1-palmitoyl-2-oleoyl-*sn*-glycero-3-phosphocholine; P/L, peptide-to-lipid ratio

* Corresponding author. Tel.: +1 212 650 8364; fax: +1 212 650 6107.
E-mail addresses: majamihajlovic@yahoo.com (M. Mihajlovic), tlazaridis@ccny.cuny.edu (T. Lazaridis).

0005-2736/$ – see front matter © 2012 Elsevier B.V. All rights reserved.
doi:10.1016/j.bbamem.2012.01.016

A different picture of antimicrobial pores emerged from computer simulations. Toroidal pores formed by the magainin analog MG-H2 and melittin in molecular dynamics simulations are disordered, with a few peptides in the center of the pore and other peptides at the pore rim [21–23]. The peptides are found in a variety of orientations with respect to the membrane surface, and rarely perpendicular to the membrane. Barrel-stave pores of alamethicin are also less ordered than in the classical view, with a water pore surrounded by tilted peptides [24,25]. Our recent MD simulations of a melittin tetramer and alamethicin tetramer and hexamer embedded into a pre-formed cylindrical or toroidal pore in a DMPC (1,2-dimyristoyl-*sn*-glycero-3-phosphocholine) bilayer also suggest that pores formed by antimicrobial peptides are irregular [26], although not as disordered as those of Sengupta et al. [23]. Possible reasons for the discrepancy may be the different initial conditions combined with limited simulation times and different force fields.

Knowing the pore structure is important because it would allow us to make predictions. We could predict, for example, the effect of specific peptide sequence changes on pore stability, and thus peptide activity. The type of the pore (cylindrical or toroidal) is an important piece of information, along with the size of the pore and the number of peptides participating. In this paper we used the same simulation strategy as in our previous study [26] to investigate the formation of pores by mutants of three antimicrobial peptides, melittin, alamethicin and MG-H2. The mutants were designed so as to obtain insight into 1) the importance of charged residues in pore formation, 2) the role of imperfect amphipathicity of AMPs in their mode of action and 3) the effect of proline on peptide structure and pore formation. Wild type melittin and MG-H2 are known to act via the toroidal pore mechanism [17,20,21,23,27,28]. In our previous MD simulations [26] as well as others reported recently [29], a melittin tetramer inserted into a pre-formed cylindrical pore transformed the pore into a semitoroidal one, with a few headgroups located within the pore region without the two leaflets meeting completely. In the present simulations, wild type MG-H2 formed a fully toroidal pore, which is more disordered than that of melittin and similar to the pores reported previously [21]. Our simulations of mutants indicate that charged residues near the N-terminus of the three peptides studied are required for toroidal pore formation. Furthermore, imperfect amphipathicity of melittin seems to facilitate formation of toroidal pores by optimizing the position of the N-terminal half so that lysine 7 can attract headgroups and "pull" them up into a pore. Finally, a proline to alanine substitution in melittin is found to affect both helix structure and pore formation.

2. Methods

2.1. Initial structures

The coordinates for melittin and alamethicin were obtained from the Protein Data Bank (PDB ID: 2MLT[30,31] and 1AMT[16], respectively). The magainin 2 analog, MG-H2 [28], was built as an ideal α-helix. The sequences of melittin, alamethicin, MG-H2 and their mutants studied here are given in Table 1. For melittin and MG-H2, the N-terminus was protonated and the C-terminus was deprotonated. The mutants of the peptides were constructed using the same initial structures by replacing the mutated side chain (shown in bold in Table 1). All charged residues were in the standard ionization state corresponding to pH ~ 7.

In principle, one should consider different protonation states. However, the charged side chains in these simulations are always in aqueous or at least polar environment, so pK_a shifts should be small. This has been confirmed experimentally in some cases. For example, the pK_as of the N-terminus and three lysines of melittin in zwitterionic micelles were found to be only slightly different from the values in phosphate buffer [32,33]. Also, the pK_a of the N-terminus of the hemagglutinin fusion peptide, which is believed to reside at the membrane–water interface, has been found to be not depressed but elevated compared to the value in water [34,35]. The elevation of pK_a has been attributed to intramolecular interactions [34]. Even for side chains buried in the membrane interior, pK_a shifts have been found smaller than expected due to water defects [36].

Table 1
Sequences of melittin, alamethicin, MG-H2 and their mutants.

Peptide	1	7	14	21
Melittin	GIGAVL	KVLTTGL	PALISWI	KRKRQQ
K7A	GIGAVL	**A**VLTTGL	PALISWI	KRKRQQ
K7Q	GIGAVL	**Q**VLTTGL	PALISWI	KRKRQQ
P14A	GIGAVL	KVLTTGL	**A**ALISWI	KRKRQQ
K23L/R24L	GIGAVL	KVLTTGL	PALISWI	KR**LL**QQ
K21F/R24L	GIGAVL	KVLTTGL	PALISWI	**F**RK**L**QQ
Alamethicin[a]	X-BPBABA	QBVBGLB	PVBBEQZ	
Q7K[a]	X-BPBABA	**K**BVBGLB	PVBBEQZ	
MG-H2	IIKKFL	HSIWKFG	KAFVGEI	MNI
K3Q/K4Q	II**QQ**FL	HSIWKFG	KAFVGEI	MNI
K11Q/K14Q	IIKKFL	HSIW**Q**FG	**Q**AFVGEI	MNI
K11Q	IIKKFL	HSIW**Q**FG	KAFVGEI	MNI
K14Q	IIKKFL	HSIWKFG	**Q**AFVGEI	MNI

[a] X = Ace, acetylated N-terminus; B = Aib, α-mehylalanine; and Z = Phl, phenylalaninol.

2.2. Simulation setup

2.2.1. Membrane with a pre-formed cylindrical pore

The simulation setup was the same as described previously [26]. The membrane with a cylindrical pore (15 Å radius) was built using membrane builder in the CHARMM-GUI website (http://www.charmm-gui.org) [37]. The system consisted of 71 DMPC lipids, 4096 water molecules (modeled as TIP3P), 7 potassium (K^+) and 7 chloride (Cl^-) ions. The miscellaneous mean-field potential was applied to keep the lipid headgroups close to their equilibrium position, ±17 Å (planar restraints), and to prevent the lipid tails from closing the pore (cylindrical restraints, the cylinder having a radius of 15 Å with its long axis along the *z* axis). After minimizing its energy, the system was equilibrated for 375 ps before a 4-ns MD simulation at constant pressure (P = 1 atm) and temperature (T = 303.15 K). Periodic boundary conditions were applied in all three dimensions, with Particle Mesh Ewald used for the calculation of electrostatics. The initial size of the primary box was 56.4 Å × 56.4 Å × 64 Å. The simulation was performed using the CHARMM software [38], with the CHARMM27 force field [39,40].

2.2.2. Peptides inserted into the pore

The last structure of the membrane with a cylindrical pore obtained at the end of the 4-ns constant pressure and temperature (CPT) MD simulation (see above) was used in the subsequent simulations of peptides inserted into the pore. Four monomers of melittin mutants, MG-H2, or MG-H2 mutants were placed in the pore, with their nonpolar face towards the lipids. Thus, the peptide-to-lipid ratio in these simulations is P/L = 4/71, which is within the range at which pores of melittin were observed [20]. The number of melittin peptides used here agrees with the experimental estimates [41–43]. Also, in previous MD simulations, at least three melittin peptides were required to form a pore in a DPPC (1,2-dipalmitoyl-*sn*-glycero-3-phosphocholine) bilayer consisting of 128 lipids [23] whereas MG-H2 pores were formed in a DPPC bilayer at P/L = 4/128 [21]. For alamethicin Q7K, six monomers were placed in the pore, which is in agreement with the estimated number of alamethicin monomers in a DMPC bilayer [44]. Hence, the peptide-to-lipid ratio in this simulation is 6/71. The same ratios were used in our previous simulations

of melittin and alamethicin [26]. The initial configuration of the peptides embedded in the cylindrical pore is shown in Figs. 1, 4, 5 and 6 (0 ns snapshot). The system was solvated in water (TIP3P) and chloride ions (Cl^-) were added to neutralize the total charge of the system. Details of the systems simulated are given in Table 2. The energy of the system was initially minimized, followed by a 575-ps equilibration and a CPT MD simulation (P = 1 atm, T = 303.15 K). Periodic boundary conditions were applied in all three dimensions, with Particle Mesh Ewald used to calculate electrostatic interactions. All simulations were performed using the NAMD software [45], with the CHARMM27 force field [39,40]. The topology and parameters for non-standard residues of alamethicin (α-methylalanine, Aib, and phenylalaninol, Phl) were developed based on similarities with serine and phenylalanine side chain. The parameters are given in Table S1 in Supplementary Data.

For data analysis, interaction energies were calculated from simulation trajectories saved every 200 ps. The energies were averaged from 80 ns until the end of the simulation. Error bars are computed as the standard deviation of four block averages. These interaction energies are high because they contain unscreened Coulomb interactions. They do not contain any entropic effects and should be used only in a qualitative sense. The COOR HBOND command in the CHARMM software [38] was used to calculate the average number of backbone i, i + 4 hydrogen bonds, which was then used to calculate the α-helicity of the peptides. The average helicity reported in Table 2 is obtained by averaging the helicity of all peptides in a system. The COOR HELIX command in CHARMM was used to calculate the helix axis of peptides from trajectories and thus the tilt angles (relative to the membrane surface normal) and the kink angles (the angle between the N-terminal and the C-terminal helices). The helix axes of alamethicin and MG-H2 were defined by the Cα atoms of residues 5 to 15 and of residues 5 to 19, respectively. For melittin, the helix axes of the N-terminal and C-terminal helices were defined by the Cα atoms of residues 1 to 10 and 13 to 26, respectively. The spherical atomic radial distribution function $g(r)$ was calculated using the g(r) GUI plugin in VMD [46].

Table 2
Summary of the MD simulations performed.[a]

Peptide	Number of monomers	Number of water molecules	Number of ions[b]	Time (ns)	Average α-helicity (%)[c]
Melittin[d]	4	3100	20	140	63 ± 2
K7A	4	3126	20	216	63 ± 2
K7Q	4	3115	16	160	64 ± 3
P14A	4	3101	20	200	71 ± 1
K23L/R24L	4	3119	12	160	63 ± 3
K21F/R24L	4	3116	12	160	63 ± 3
Alamethicin[d]	6	3113	6	160	55 ± 4
Q7K	6	3118	0	160	56 ± 2
MG-H2	4	3128	16	160	59 ± 5
K3Q/K4Q	4	3141	8	136	63 ± 5
K11Q/K14Q	4	3141	8	160	50 ± 3
K11Q	4	3133	12	160	62 ± 4
K14Q	4	3135	12	160	65 ± 3

[a] Each system contains 71 DMPC lipids.
[b] K^+ in the case of alamethicin, otherwise Cl^-.
[c] Averaged over all peptides in the system.
[d] Reported in [26].

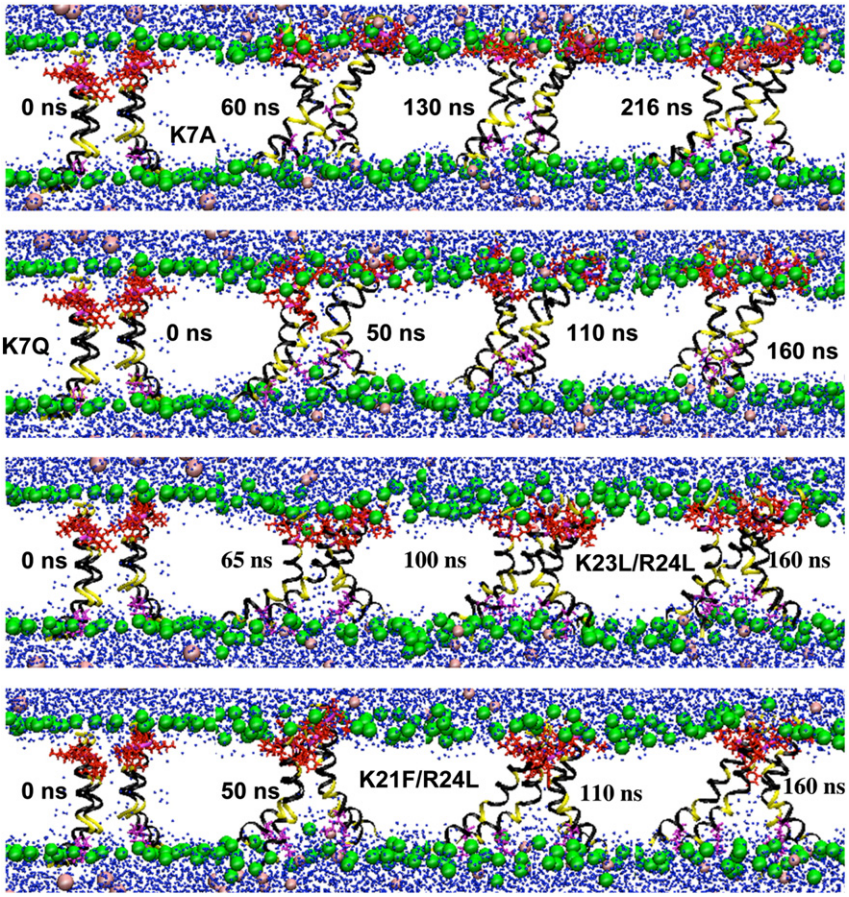

Fig. 1. Snapshots from MD simulations of melittin K7A, K7Q, K23L/R24L and K21F/R24L tetramers inserted into a pre-formed cylindrical pore (0 ns snapshots). The phosphocholines are shown as green balls, water as blue balls, Cl^- ions as pink balls, residue 7 as magenta licorice, residues 21, 22, 23 and 24 as red licorice, and the peptides as ribbons with the nonpolar residues colored in black, the polar residues colored in yellow, and the charged residues colored in magenta; the lipid tails have been removed for clarity.

In the simulations, a pore is considered to be fully toroidal if headgroups from the upper and lower leaflet seem to be connected, semitoroidal if headgroups in the vicinity of the pore are perturbed from their equilibrium position, headgroups enter the pore region transiently and the overall shape of the pore is curved, and cylindrical (barrel-stave) if headgroups are located exclusively at the membrane surface.

3. Results

3.1. Melittin K7A, K7Q, K21F/R24L and K23L/R24L mutants

We have previously performed a 140-ns MD simulation of a melittin tetramer embedded in a pre-formed cylindrical pore [26]. Initially, the peptides were in a transmembrane orientation, with their C-termini at the upper leaflet and the N-termini at the lower leaflet. By the end of the simulation, the peptides assumed tilted transmembrane orientations and an initially cylindrical pore changed to a semitoroidal one, with headgroups from the two leaflets entering the interior of the pore, but not meeting completely as they would in a toroidal pore (Fig. 2B in [26] and the 'MLT' snapshot in Fig. 3). It appeared that lysine 7, located near the N-terminus of melittin, initialized the formation of a toroidal pore by perturbing headgroups in the lower leaflet and "pulling" them up into the pore. Other studies also indicated the importance of K7 for pore formation [47,48] and hemolytic activity of melittin [49].

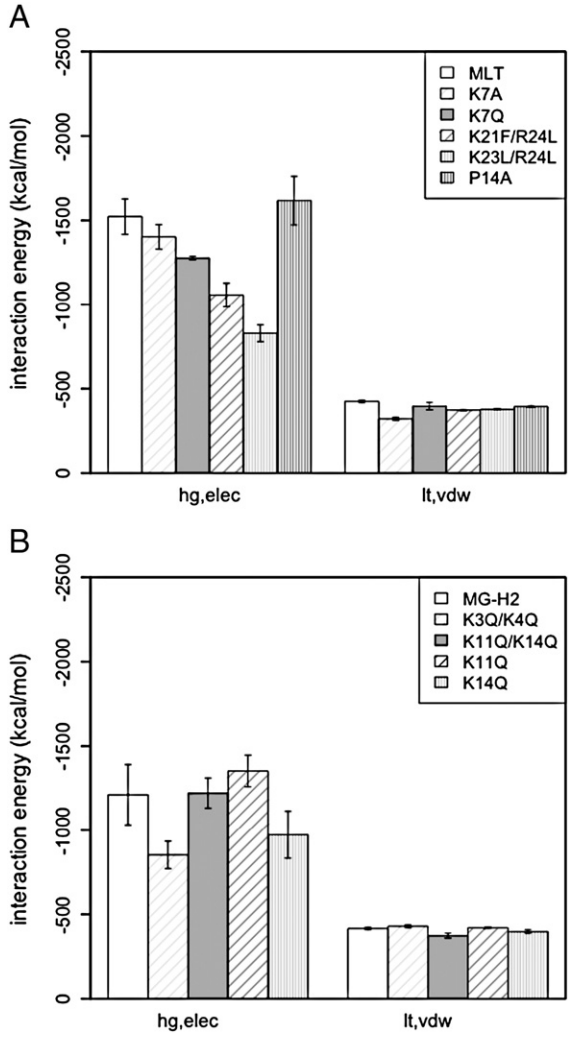

Fig. 2. (A) Interaction energy of melittin (MLT) and its mutants with lipids. (B) Interaction energy of MG-H2 and its mutants with lipids. 'Elec' stands for electrostatic interactions, 'vdw' for Van der Waals interactions, 'hg' for headgroups, and 'lt' for lipid tails.

Thus, to investigate the role of K7 in pore formation, we constructed melittin mutants with K7 replaced with alanine (K7A) or glutamine (K7Q). Fig. 1 shows snapshots from the MD simulations of the mutants started in a pre-formed cylindrical pore. In contrast to melittin, the mutants did not reshape the cylindrical pore during the simulations. These results suggest that having a polar residue (glutamine) instead of a charged one (lysine) near the N-terminus of melittin is not enough to produce a toroidal pore. The calculated peptide–lipid interactions in the pores are reduced compared to melittin, especially electrostatic interactions with the lipid headgroups (Fig. 2A). On the other hand, the interactions of the mutants with the lipid tails are not much affected. Therefore, a charged residue near the N-terminus of melittin indeed seems to be required to initialize the formation of toroidal pores.

In a previous study, we noted that antimicrobial peptides often have imperfectly amphipathic structure, with a few polar or charged residues in the nonpolar face, which may interfere with binding to a flat membrane [50]. Here, we designed a melittin mutant with K23 and R24 substituted by leucine to test this hypothesis. According to a helical wheel, K23 and R24 are located in the nonpolar face of the helix [51]. The snapshots from an MD simulation of a melittin K23L/R24L tetramer inserted into an initially cylindrical pore are shown in Fig. 1. The pore remained cylindrical until the end of the 160-ns simulation. The interaction energy between the peptides and lipids is significantly less favorable than for melittin, mostly due to a loss of electrostatic interactions (Fig. 2A). Although the mutant has two extra leucines instead of two positively charged residues in the nonpolar face, its hydrophobic interactions with the lipid tails did not change compared to melittin.

Another melittin mutant tested has K21 and R24 replaced with phenylalanine and leucine, respectively. Lysine 21 is located at the interface between polar and nonpolar faces of the melittin helix [51]. This mutant has a broader nonpolar face than melittin, with only one charged residue (K23). Again, the mutations suppressed the formation of a toroidal pore. Until the end of the 160-ns MD simulation, the pore remained cylindrical (Fig. 1). Similar to melittin K23L/R24L, the interaction energy between melittin K21F/R24L and lipids is considerably reduced compared to melittin (Fig. 2A).

Fig. 3 shows the configuration of pores at the end of the MD simulations (peptides and ions are removed for clarity). Although only one headgroup can be seen in the MLT snapshot shown in Fig. 3, at earlier simulation times more headgroups were observed to enter the pore region [26]. Also, given that the lower leaflet headgroups are perturbed from their equilibrium position and that the water pore is curved, we consider this to be a semitoroidal pore. In contrast, the pores formed by the mutants (K7A, K7Q, K23L/R24L and K21F/R24L) are cylindrical and their radii are notably smaller compared to melittin. All the simulations were started from the same initial pore configuration and the location of the peptides. Previous MD simulations of a melittin monomer inserted into a DPPC bilayer in transmembrane orientation and of a melittin tetramer inserted into a POPC bilayer indicated that the protonated N-terminus and lysine 7 facilitate water penetration into the bilayer [47,48]. Bachar and Becker observed that a melittin monomer induces water penetration from both extracellular and intracellular side of the membrane and calculated that lysine 7 is the only residue whose dipole points up towards the extracellular membrane surface and attracts water within the bilayer [47]. In line with these findings, our simulations indicate that water flow into the pore is obstructed without lysine 7 (as in the K7A and K7Q mutants) or if K7 is not optimally positioned in the pore (as in the K23L/R24L and K21F/R24L mutants).

Both wild type melittin and the mutants (K7A, K7Q, K23L/R24L and K21F/R24L) are helical with a kink at P14. The calculated α-helicity of

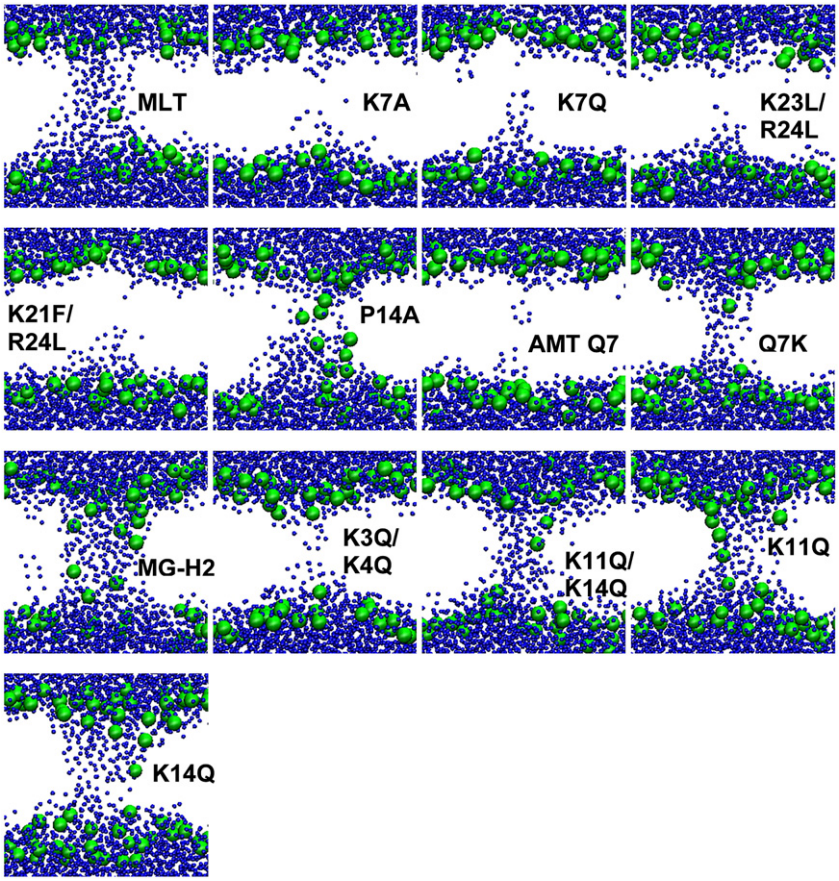

Fig. 3. Pores at the end of MD simulations: melittin (MLT) at 140 ns, K7A at 216 ns, K7Q, K23L/R24L and K21F/R24L at 160 ns, P14A at 200 ns; alamethicin (AMT Q7) and Q7K at 160 ns; MG-H2 at 160 ns, K3Q/K4Q at 136 ns, and K11Q/K14Q, K11Q and K14Q at 160 ns. The peptides and ions are removed for clarity. The phosphocholines are shown as green balls and water as blue balls.

the peptides during the MD simulations is ~63% (Table 2). The kink angle of the mutants is similar to that of melittin whereas the tilt angles of the N-terminal and C-terminal helices, with respect to the membrane surface normal, are somewhat different (Fig. S1). Although the peptides assume a wide range of tilt angles, the N-terminal halves of K23L/R24L and K21F/R24L are, on average, more tilted than melittin. This places lysine 7 closer to the membrane surface (Fig. 1, K7 is shown as magenta licorice), which may preclude the entry of headgroups into the pore region and thus interfere with the formation of a toroidal pore. The more tilted N-terminal helices are likely a consequence of optimizing the position of residues F21, L23 and L24 so that they are located in a hydrophobic environment. In Fig. 1, these residues are shown as red licorice and it can be seen that they are oriented towards the lipid tails (in K23L/R24L) or at the peptide–peptide interface (in K21F/R24L).

The mutations affect peptide–peptide interactions, as shown in Fig. S2. In general, the Van der Waals interaction energy is more favorable for the mutants than for melittin, but the electrostatic repulsions tend to be larger for the mutants, despite the charge reduction. This is likely so because their pores are narrower than the melittin pore (Fig. 3) and the mutants are more tightly packed than the melittin peptides (Fig. S3A). In the mutants, residues 7, 21, 22, 23 and 24 are in a closer contact with each other than in the melittin tetramer (Figs. S3B and C), which evidently increases peptide–peptide repulsions.

3.2. Melittin P14A mutant

It has been reported that substitution of proline 14 by alanine resulted in stronger binding affinity for POPC (1-palmitoyl-2-oleoyl-*sn*-glycero-3-phosphocholine) membranes, less efficient leakage of fluorescent markers, different pore formation kinetics and different hemolytic mechanisms [52–54]. These differences have been attributed to structural changes brought about by the mutation. Proline is known to decrease α-helicity and increase flexibility of helices. Here we look at how the mutation P14A affects pore formation.

Fig. 4A shows snapshots from a 200-ns MD simulation of a melittin P14A tetramer inserted into an initially cylindrical pore. Soon after the onset of the simulation, headgroups start to enter into the pore region (18 ns snapshot). At ~100 ns, headgroups from the two leaflets connect but the peptides are located at only one side of the pore, which contrasts with the melittin pore [26]. This configuration is maintained until the end of the simulation (200 ns snapshot). As Fig. 4B shows, at the end of the simulation, three peptides are oriented with their polar faces facing each other and the nonpolar faces next to the lipids. Lysine 7 of two peptides (peptides 1 and 2) point towards the interior of the aggregate and are solvated in water while lysine 7 of the third peptide (peptide 3) points towards the lower leaflet headgroups. The fourth peptide (peptide 4) reoriented so that its polar face is next to the headgroups located within the bilayer. This is likely a metastable stable state and, at longer times, the headgroups would move from the bilayer interior to the surface.

The calculated melittin P14A–lipid interaction energy is comparable to that of melittin, within the error (Fig. 2A). The proline to alanine substitution decreases the kink angle between the N-terminal and C-terminal helices and changes the tilt angles of the helices relative to the membrane surface (Fig. S1). The α-helicity is also affected by the mutation, being higher in the mutant than in melittin (Table 2). Yet, the calculated α-helicity of P14A in the pore is smaller than the experimentally determined helicity of a monomeric peptide

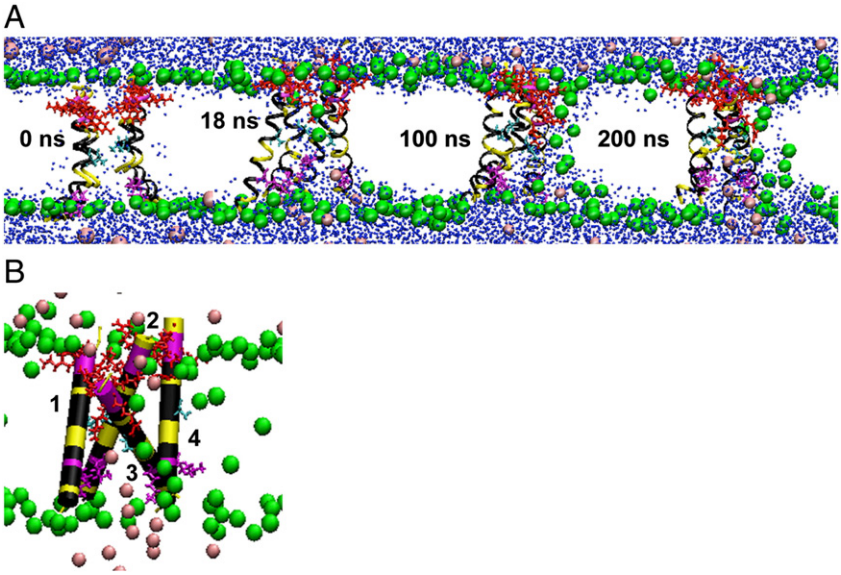

Fig. 4. (A) Snapshots from a MD simulation of a melittin P14A tetramer inserted into a pre-formed cylindrical pore (0 ns snapshot). The phosphocholines are shown as green balls, water as blue balls, Cl^- ions as pink balls, the peptides as ribbons with the nonpolar residues colored in black, the polar residues colored in yellow and the charged residues colored in magenta; the lipid tails have been removed for clarity. Residue 7 is shown as magenta licorice, residues 21, 22, 23 and 24 as red licorice and residue 14 as cyan licorice. (B) Orientation of the helices at 200 ns. K7 and A14 are located in the polar face.

bound to POPC vesicles, $93 \pm 7\%$ [53]. In the P14A tetramer, there are stronger electrostatic repulsions between the peptides than in melittin, even though their net charge is the same (Fig. S2). On the other hand, the Van der Waals interactions are more favorable. This is likely due to different peptide arrangements. Fig. S3 shows that the P14A peptides are closer to each other than the melittin peptides, especially the charged residues K21, R22, K23 and R24.

3.3. Alamethicin Q7K mutant

In our previous MD simulations, we have observed that an alamethicin hexamer prefers cylindrical to toroidal pores and that glutamine 7 located inside the pore provides a hydrophilic environment for pore water [26]. Since a charged residue near the N-terminus of melittin (K7) seems to be important for toroidal pore formation, we constructed an alamethicin mutant with Q7 substituted by lysine to see whether it will affect pore formation. Fig. 5 shows the snapshots from a 160-ns MD simulation of an alamethicin Q7K hexamer embedded in an initially cylindrical pore. The configuration of pores shown is quite different from that of the pores formed by alamethicin (Fig. S1C in [26] and 'AMT Q7' and 'Q7K' snapshots in Fig. 3). During the simulation, two peptides changed their initially transmembrane orientations to one almost parallel to the membrane surface and moved towards the brink of the pore. The other four peptides lined the pore but are in a

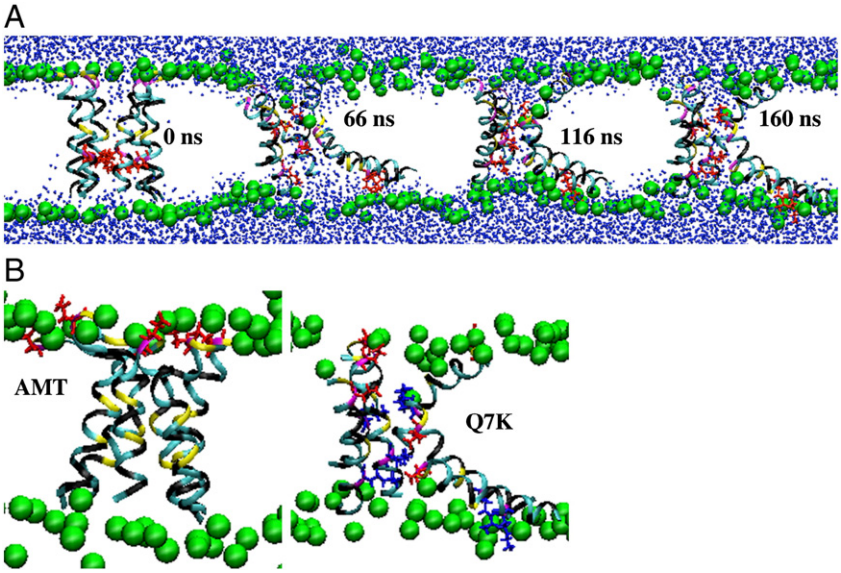

Fig. 5. (A) Snapshots from a MD simulation of an alamethicin Q7K hexamer inserted into a pre-formed cylindrical pore (0 ns snapshot). The phosphocholines are shown as green balls, water as blue balls, K7 as red licorice, and the peptides as ribbons with the nonpolar residues colored in black, the polar residues colored in yellow, the charged residues colored in magenta and the nonstandard residues (Aib and Phl) in cyan; the lipid tails have been removed for clarity. (B) Glutamate (red licorice) interacting with phosphocholines and/or lysine (blue licorice), at the end of the simulations of alamethicin (AMT) and alamethicin Q7K.

more tilted transmembrane orientation than the wild type peptides (Fig. S5A). Also, the lower and upper leaflet headgroups are perturbed from their equilibrium position and a few headgroups enter the pore region during the simulation (66 ns and 116 ns snapshots), giving the pore a curved appearance. The calculated average interaction energies between the peptides and headgroups are similar for the mutant and wild type (the average electrostatic interactions, which predominate, are: -457 ± 53 and -442 ± 48 kcal/mol, respectively). A large portion of these interactions comes from the interaction between the OE1 or OE2 atoms of glutamate (E18) and the N atom of lipid cholines (for alamethicin, -157 ± 56 kcal/mol, and for the mutant, -214 ± 77 kcal/mol). Fig. 5B shows how glutamates (red licorice) interact with headgroups at the end of the simulations. The peptide–lipid tail interactions, mostly due to the Van der Waals interactions, are somewhat more favorable for the mutant (Q7K: -415 ± 9 kcal/mol, AMT: -358 ± 10 kcal/mol). The α-helicity of the mutant is comparable to that of alamethicin (Table 2).

The peptide–peptide electrostatic interactions are more favorable in the mutant than in alamethicin whereas the Van der Waals interactions are comparable (Fig. S4). In the mutant, there are significant interactions between glutamates (E18) and lysines (K7), as illustrated in Fig. 5B. The averaged electrostatic interaction energy between Glu and Lys is -374 ± 58 kcal/mol.

3.4. MG-H2 and mutants

We performed a 160-ns MD simulation of a MG-H2 tetramer inserted into a pre-formed cylindrical pore. Soon after the beginning of the simulation, two peptides changed their orientation from an initially transmembrane to a tilted orientation (Fig. S5B) and moved towards the edges of the pore. At the same time, headgroups from the two leaflets started to enter the pore region and the pore assumed a toroidal shape (Fig. 6, 24 ns and 72 ns snapshots). Such a pore configuration remained until the end of the simulation (Fig. 3). The pores observed in our simulation are similar to the previously reported disordered toroidal pores of MG-H2, with only one or two peptides found in the center of the pore and the others at the pore rim [21].

Although both melittin and MG-H2 form toroidal pores, the pores differ significantly. Both peptides have a positive net charge at pH~7

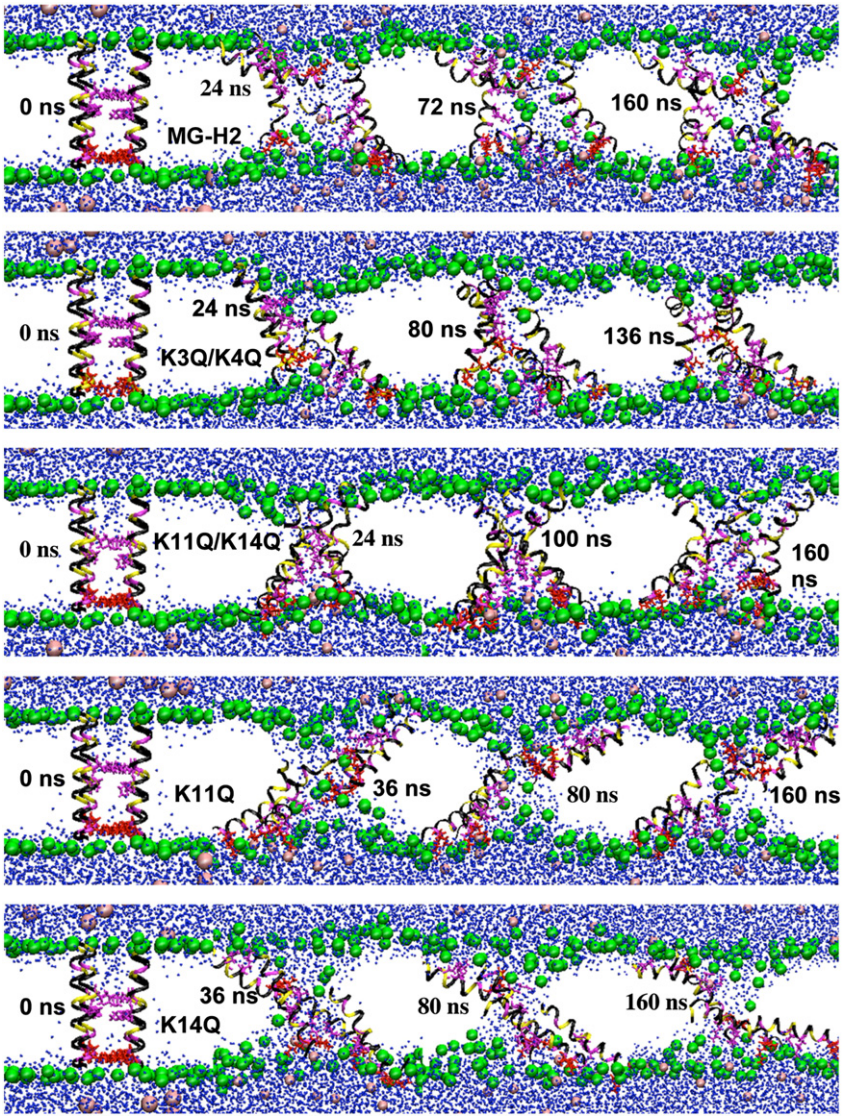

Fig. 6. Snapshots from MD simulations of a MG-H2, K3Q/K4Q, K11Q/K14Q, K11Q and K14Q tetramer inserted into a pre-formed cylindrical pore (0 ns snapshots). The phosphocholines are shown as green balls, water as blue balls, Cl^- ions as pink balls, the peptides as ribbons with the nonpolar residues colored in black, the polar residues colored in yellow and the charged residues colored in magenta; the lipid tails have been removed for clarity. Residues 3 and 4 are shown as red licorice while residues 11 and 14 are shown as magenta licorice.

(melittin +5, MG-H2 +4), but the charged residues are differently distributed along the helix. Melittin has one lysine near the N-terminus (K7) and two lysines and two arginines near the C-terminus (K21, R22, K23 and R24) whereas MG-H2 has two lysines near the N-terminus (K3 and K4) and two lysines in the middle of the helix (K11 and K14). We hypothesize that this difference is responsible for the different pore configurations. To test this, we designed MG-H2 mutants with some of the lysines replaced with glutamine.

The first mutant tested has K3 and K4 substituted by glutamine (K3Q/K4Q). During a 136-ns MD simulation, a K3Q/K4Q tetramer initially embedded into a cylindrical pore produced a disordered pore (Fig. 6). The peptides are found in a variety of orientations with respect to the membrane surface (Fig. S5). The two leaflets are bent but they did not meet. However, since headgroups transiently enter and exit the pore region (Fig. 6, 24 ns and 80 ns snapshots), we consider the pore to be semitoroidal. Fig. 3 shows that the radius of the pore is notably smaller than that of the MG-H2 pore. The electrostatic (and total) interaction energy between peptides and headgroups is significantly more unfavorable than in the MG-H2 pore whereas the hydrophobic interactions with the lipid tails are similar (Fig. 2B). Besides the interactions between lysines and lipid phosphates, the interactions between glutamate (E19) and lipid cholines also contribute to the interaction energies. For MG-H2, the electrostatic interaction energy between the OE1 or OE2 atom of E19 and the N atom of cholines is -102 ± 46 kcal/mol whereas for K3Q/K4Q the energy is -139 ± 16 kcal/mol. The peptide–peptide electrostatic interactions are similar to those for the MG-H2 tetramer (Fig. S6). Thus, as in the case of melittin, charged residues near the N-terminus are important for the formation of a toroidal pore.

A rather different pore configuration was generated upon substitutions of K11 and K14 by glutamine (K11Q/K14Q). These two residues are located in the middle of the helix, with K11 in the center of the polar face and K14 at the interface between polar and nonpolar faces (for a helical wheel see ref. [28]). As Fig. 6 shows, the pore is less disordered and more similar to the melittin pore (Fig. 3). Here, all four peptides are in a tilted transmembrane orientation (Fig. S5B). However, the peptide–peptide electrostatic interactions are significantly more unfavorable compared to those in MG-H2, as well as in the other mutants (Fig. S6). In MG-H2, there are favorable interactions between glutamates (E19) and lysines (-239 ± 48 kcal/mol), which are absent in the mutant since the peptides are less tilted. On the other hand, the interactions with headgroups and lipid tails are similar to the interactions calculated for MG-H2 (Fig. 2B), including the interactions between glutamates and cholines (the electrostatic interaction energy between the OE1 or OE2 atom of E19 and the N atom of cholines is -129 ± 29 kcal/mol for the mutant and -102 ± 46 kcal/mol for MG-H2). The α-helicity of K11Q/K14Q is a bit lower than that of MG-H2 and the other mutants (Table 2). This simulation suggests that the charges in the middle of the helix (K11 and K14) are not essential for toroidal pore formation.

A mutation of one of two middle lysines to glutamine (K11Q and K14Q) again produced highly disordered toroidal pores (Figs. 6 and 3), with the peptides in tilted orientations and some of them almost parallel to the membrane surface (Fig. S5B). The peptide–peptide interactions are similar to those for MG-H2 (Fig. S6). In K14Q, the glutamate–lysine interactions (-323 ± 30 kcal/mol) are more favorable than in K11Q (-151 ± 13 kcal/mol) and MG-H2 (-239 ± 48 kcal/mol). On the other hand, K11Q interacts with headgroups similarly to MG-H2 but more favorably than K14Q (Fig. 2B). The electrostatic interactions between glutamates in K11Q and K14Q and lipid cholines are -71 ± 22 kcal/mol and -162 ± 25 kcal/mol. Hence, it seems that having a charged residue in the middle of the polar face (K11) brings about more disorder and decreases electrostatic interactions with headgroups.

4. Discussion

This paper reports atomistic MD simulations of melittin and alamethicin mutants, as well as MG-H2 and its mutants, designed to investigate the influence of imperfect amphipathicity and charge distribution on pore formation. All simulations were started with the peptides (tetramers, or in the case of alamethicin, hexamer) in a transmembrane orientation inserted into a pre-formed cylindrical pore. Although the simulations are fairly long, there is no guarantee that they have reached equilibrium. In fact, in one system there are strong indications that this is not the case. Ideally, the simulations should be run longer and repeated several times using different initial conditions. This is left for future work. Here we attempt to extract plausible ideas from the data obtained so far.

A mean-field study by Zemel et al. predicted that only weakly charged peptides (such as alamethicin) can form barrel-stave (i.e., cylindrical) pores whereas more charged peptides (such as melittin and MG-H2) form toroidal pores and that the pore size depends on the charge of the peptides [55]. Although the net charge of the melittin mutants studied here ($z_p=+4$ for K7A and K7Q, $z_p=+3$ for K21F/R24L and K23L/R24L) is reduced compared to melittin ($z_p=+5$), it is still above the threshold ($z_p=1$) over which the theory predicts toroidal pore formation. This contradicts our results. A probable reason for the discrepancy is that the theory assumes a uniform distribution of the peptide charges, which in not the case for the mutants tested here. Our simulations show that not only the net charge but also the distribution of charges is an important determinant for pore shape.

The MD simulations suggest that the charge in the N-terminal part of the peptide helices is required for the formation of toroidal pores. This has been observed both for melittin and MG-H2 mutants. When lysine 7 in the N-terminal half of melittin was replaced with glutamine or alanine, an initially cylindrical pore did not evolve into a toroidal pore despite the charged residue in the C-terminal half, K21, R22, K23 and R24. For MG-H2, a mutation of lysines 3 and 4 (K3Q/K4Q) resulted into a semitoroidal pore, quite different from the MG-H2 toroidal pore. Furthermore, when Q7 of alamethicin was substituted by lysine, the pore changed to semitoroidal during the simulation. An important role of lysine 7 of melittin for pore formation and anion transport [42,47,48] as well as a 74% loss in hemolytic activity of a melittin mutant with K7 omitted [49] have been reported before. Our study may provide a rationale for the latter. The simulations reveal that the K7A and K7Q mutations change the mechanism of action of melittin, resulting in notably smaller pores, which may interfere with hemoglobin and ion transport.

The residues in the middle of MG-H2 helix appear not to be essential for the formation of toroidal pores, but we found that they introduce higher disorder of the pores. Melittin does not have charged residues in the middle and this might be the reason why melittin and MG-H2 pores differ. In the melittin pore, all four peptides are in a tilted transmembrane orientation whereas in the MG-H2 pore only two peptides are located in the pore and the other two are at the pore edges. Similar MG-H2 pores were previously reported [21,22]. Although a more systematic study is necessary to draw conclusions, our simulations imply that peptides with charged residues near the N-terminus but not in the middle of the helix may form toroidal pores lined with the peptides in a variety of tilted transmembrane orientations while peptides also having charged residues in the middle of the helix may form more disordered pores.

Another interesting feature of antimicrobial peptides probed here is how their imperfect amphipathicity influences the preference for a certain pore type. Melittin has two charged residues in its nonpolar face, K23 and R24. We replaced these two residues with leucine and observed that the mutant (K23L/R24L) did not change an initially cylindrical pore into a toroidal one. The radius of the pore formed is notably smaller than that of the melittin pore. To shield leucines

from headgroups and water, the peptides assumed slightly different tilted orientations than the wild type peptides. This tilting placed K7 closer to the lower leaflet headgroups, which on the other hand, precluded the entry of headgroups into the pore region and, thus, stunted the formation a toroidal pore. A similar scenario has been seen in a simulation of another melittin mutant, K21F/R24. Taking our results together, it appears that both the charge in the N-terminal part of the melittin helix and its imperfect amphipathicity are necessary to form toroidal pores. Clearly, tests of this idea with other peptides are needed before a safe conclusion can be reached.

Proline is often found in antimicrobial peptides and ion channel forming peptides [16,43,56]. Proline disrupts α-helicity, introduces a kink in α-helices and thus increases the flexibility of peptides [57]. We performed a MD simulation of melittin with proline 14 substituted by alanine to investigate its effect on pore formation. The mutation straightened the helices and increased α-helicity. During the 200-ns simulation, melittin P14A formed a metastable state in which the peptides were located only at one side of the "pore" whereas the other side was lined with headgroups. Such a structure has not been observed for melittin. Different pore formation kinetics and hemolytic mechanisms, as well as reduced leakage and a slightly reduced hemolytic activity of P14A compared to melittin have been reported in experimental studies [49,52–54].

The calculated average α-helicity of melittin (63 ± 2%) and MG-H2 (59 ± 5%) in our simulations is higher than the helicity reported in previous MD simulations that studied their pores. For melittin, the α-helicity was reported to be 40–50% in a DPPC bilayer [23] or 35–60% in a pre-formed pore in a POPC bilayer (when the melittin peptides were arranged in asymmetric orientation, as in our simulation) [29], while for MG-H2 in a DPPC bilayer it was 15–50% [21]. It could be that the discrepancies in the calculated α-helicities are due to different initial simulation conditions, but also to differences in force fields [58]. The α-helicity determined from circular dichroism experiments also varies significantly. For melittin it is reported to be 27% in the presence of DMPC [59], 47% in the presence of PC/Chol (phophatidylcholine/cholesterol) vesicles [60] and ~50% for MG-H2 in PC [28].

Although DMPC lipids are not a major component in bacterial cell membranes, they are commonly used in in vitro biophysical studies. For example, it has been shown that melittin forms tetrameric aggregates in a DMPC membrane, arranged in accordance with the pore model [43]. It is possible, however, that the structure of the pore might be somewhat different in thicker membranes, such as POPC or DPPC. For instance, it has been determined that alamethicin adopts a transmembrane orientation both in POPC and DMPC membranes, but it is more tilted in a DMPC bilayer [61]. It would be interesting to repeat these studies with longer and more physiologically relevant lipids.

The simulations presented in this paper indicate that charged distribution and imperfect amphipathicity of antimicrobial peptides play an important role in pore formation and can contribute to a better understanding of mechanism of action of antimicrobial peptides. However, the results need to be confirmed by experiments as well as in additional MD simulations on a larger number of peptides. Since we have tested pore formation of antimicrobial peptides in a zwitterionic membrane, it would be interesting to see how their hemolytic activity and leakage ability correlate to our findings. Also, given that melittin and magainin bind more strongly to anionic lipids, it remains for future computer simulations to probe pore formation by the mutants in anionic membranes.

Acknowledgements

This work was supported by the National Science Foundation (MCB-0615552) and NIH (SC1GM087190). Infrastructure support was provided in part by RCMI grant RR03060 from NIH. A grant of computer time from the City University of New York High Performance Computing Center supported under NSF Grants CNS-0855217 and CNS-0958379 is also acknowledged.

Appendix A. Supplementary data

Supplementary data to this article can be found online at doi:10.1016/j.bbamem.2012.01.016.

References

[1] K. Brogden, Antimicrobial peptides: pore formers or metabolic inhibitors in bacteria? Nat. Rev. Microbiol. 3 (2005) 238–250.
[2] K.L. Brown, R.E.W. Hancock, Cationic host defense (antimicrobial) peptides, Curr. Opin. Immunol. 18 (2006) 24–30.
[3] R.E.W. Hancock, Cationic peptides: effectors in innate immunity and novel antimicrobials, Lancet Infect. Dis. 1 (2001) 156–164.
[4] B. Bechinger, Structure and function of membrane-lytic peptides, Crit. Rev. Plant Sci. 23 (2004) 271–292.
[5] A.M. Cole, Antimicrobial peptide microbicides targeting HIV, Protein Pept. Lett. 12 (2005) 41–47.
[6] K. Matsuzaki, Control of cell selectivity of antimicrobial peptides, Biochim. Biophys. Acta 1788 (2009) 1687–1692.
[7] N. Papo, Y. Shai, Host defense peptides as new weapons in cancer treatment, Cell. Mol. Life Sci. 62 (2005) 784–790.
[8] U. Silphaduang, E.J. Noga, Peptide antibiotics in mast cells of fish, Nature 414 (2001) 268–269.
[9] Y. Li, The role of antimicrobial peptides in cardiovascular physiology and disease, Biochem. Biophys. Res. Commun. 390 (2009) 363–367.
[10] J.P. Bradshow, Cationic antimicrobial peptides. Issues for potential clinical use, BioDrugs 17 (2003) 233–240.
[11] K. Matsuzaki, Why and how are peptide–lipid interactions utilized for self-defense? Magainins and tachyplesins as archetypes, Biochim. Biophys. Acta 1462 (1999) 1–10.
[12] K. Matsuzaki, K. Sugishita, N. Fujii, K. Miyajima, Molecular basis for membrane selectivity of an antimicrobial peptide, magainin 2, Biochemistry 34 (1995) 3423–3429.
[13] H.W. Huang, Molecular mechanism of antimicrobial peptides: the origin of cooperativity, Biochim. Biophys. Acta 1758 (2006) 1292–1302.
[14] Z. Oren, Y. Shai, Mode of action of linear amphipathic alpha-helical antimicrobial peptides, Biopoly. 47 (1998) 451–463.
[15] K. He, S.J. Ludtke, D.L. Worcester, H.W. Huang, Neutron scattering in the plane of membranes: structure of alamethicin pores, Biophys. J. 70 (1996) 2659–2666.
[16] R.O. Fox Jr., F.M. Richards, A voltage-gated ion channel model inferred from the crystal structure of alamethicin at 1.5-Å resolution, Nature 300 (1982) 325–330.
[17] D. Allende, S.A. Simon, T.J. McIntosh, Melittin-induced bilayer leakage depends on lipid material properties: evidence for toroidal pores, Biophys. J. 88 (2005) 1828–1837.
[18] S.J. Ludtke, K. He, W.T. Heller, T.A. Harroun, L. Yang, H.W. Huang, Membrane pores induced by magainin, Biochemistry 35 (1996) 13723–13728.
[19] K. Matsuzaki, O. Murase, N. Fujii, K. Miyajima, An antimicrobial peptide, magainin 2, induced rapid flip-flop of phospholipids coupled with pore formation and peptide translocation, Biochemistry 35 (1996) 11361–11368.
[20] L. Yang, T.A. Harroun, T.M. Weiss, L. Ding, H.W. Huang, Barrel-stave model or toroidal model? A case study on melittin pores, Biophys. J. 81 (2001) 1475–1485.
[21] H. Leontiadou, A.E. Mark, S.J. Marrink, Antimicrobial peptides in action, J. Am. Chem. Soc. 128 (2006) 12156–12161.
[22] A.J. Rzepiela, D. Sengupta, N. Goga, S.J. Marrink, Membrane poration by antimicrobial peptides combining atomistic and coarse-grained descriptions, Faraday Discuss. 144 (2010) 431–443.
[23] D. Sengupta, H. Leontiadou, A.E. Mark, S.J. Marrink, Toroidal pores formed by antimicrobial peptides show significant disorder, Biochim. Biophys. Acta 1778 (2008) 2308–2317.
[24] L. Thøgersen, B. Schiøtt, T. Vosegaard, N.C. Nielsen, E. Tajkhorshid, Peptide aggregation and pore formation in a lipid bilayer: a combined coarse-grained and all atom molecular dynamics study, Biophys. J. 95 (2008) 4337–4347.
[25] D.P. Tieleman, B. Hess, M.S.P. Sansom, Analysis and evaluation of channel models: simulations of alamethicin, Biophys. J. 83 (2002) 2393–2407.
[26] M. Mihajlovic, T. Lazaridis, Antimicrobial peptides in toroidal and cylindrical pores, Biochim. Biophys. Acta 1798 (2010) 1485–1493.
[27] K. Matsuzaki, S. Yoneyama, K. Miyajima, Pore formation and translocation of melittin, Biophys. J. 73 (1997) 831–838.
[28] T. Tachi, R.F. Epand, R.M. Epand, K. Matsuzaki, Position-dependent hydrophobicity of the antimicrobial magainin peptide affects the mode of peptide–lipid interactions and selective toxicity, Biochemistry 41 (2002) 10723–10731.
[29] S.J. Irudayam, M.L. Berkowitz, Influence of the arrangement and secondary structure of melittin peptides on formation and stability of toroidal pores, Biochim. Biophys. Acta 1808 (2011) 2258–2266.
[30] T.C. Terwilliger, D. Eisenberg, The structure of melittin. I. Structure determination and partial refinement, J. Biol. Chem. 257 (1982) 6010–6015.
[31] T.C. Terwilliger, D. Eisenberg, The structure of melittin. II. Interpretation of the structure, J. Biol. Chem. 257 (1982) 6016–6022.
[32] L. Zhu, M.D. Kemple, P. Yuan, F.G. Prendergast, N-terminus and lysine side chain pK_a values of meilttin in aqueous solutions and micellar dispersions measured by ^{15}N NMR, Biochemistry 34 (1995) 13196–13202.

[33] B. Stanislawski, H. Rüterjans, ^{13}C-NMR investigation of the insertion of the bee venom melittin into lecithin vesicles, Eur. Biophys. J. 15 (1987) 1–12.
[34] J.L. Lorieau, J.M. Louis, A. Bax, Helical hairpin structure of influenza hemagglutinin fusion peptide stabilized by charge–dipole interactions between the N-terminal amino group and the second helix, J. Am. Chem. Soc. 133 (2011) 2824–2827.
[35] Z. Zhou, J.C. Macosko, D.W. Hughes, B.G. Sayer, J. Hawes, R.M. Epand, ^{15}N NMR study of ionization properties of the influenza virus fusion peptide in zwitterionic phospholipid dispersions, Biophys. J. 78 (2000) 2418–2425.
[36] L. Li, I. Vorobyov, T.W. Allen, Potential of mean force and pK_a profile calculation for a lipid membrane-exposed arginine side chain, J. Phys. Chem. B 112 (2008) 9574–9587.
[37] S. Jo, T. Kim, W. Im, Automated builder and database of protein/membrane complexes for molecular dynamics simulations, PLoS One 2 (2007) e880.
[38] B.R. Brooks, C.L. Brooks III, A.D. MacKerell Jr., L. Nilsson, R.J. Petrella, B. Roux, Y. Won, G. Archontis, C. Bartels, A. Boresch, A. Caflisch, L. Caves, Q. Cui, A.R. Dinner, M. Feig, S. Fischer, J. Gao, M. Hodoscek, W. Im, K. Kuczera, T. Lazaridis, J. Ma, V. Ovchinnikov, E. Paci, R.W. Pastor, C.B. Post, J.Z. Pu, M. Schaefer, B. Tidor, R.M. Venable, H.L. Woodcock, X. Wu, W. Yang, D.M. York, M. Karplus, CHARMM: the biomolecular simulation program, J. Comput. Chem. 30 (2009) 1545–1614.
[39] A.D. MacKerell Jr., D. Bashford, M. Bellott, R.L. Dunbrack Jr., J.D. Evanseck, M.J. Field, S. Fischer, J. Gao, H. Guo, S. Ha, D. Joseph-McCarthy, L. Kuchnir, K. Kuczera, F.T.K. Lau, C. Mattos, S. Michnick, T. Ngo, D.T. Nguyen, B. Prodhom, W.E. Reiher III, B. Roux, M. Schlenkrich, J.C. Smith, R. Stote, J. Straub, M. Watanabe, J. Wiorkiewicz-Kuczera, D. Yin, M. Karplus, All-atom empirical potential for molecular modeling and dynamics studies of proteins, J. Phys. Chem. B 102 (1998) 3586–3616.
[40] A.D. MacKerell Jr., M. Feig, C.L. Brooks III, Extending the treatment of backbone in protein force fields: limitations of gas-phase quantum mechanics in reproducing protein conformational distributions in molecular dynamics simulations, J. Comput. Chem. 25 (2004) 1400–1415.
[41] M.T. Tosteson, O. Alvarez, W. Hubbell, R.M. Bieganski, C. Attenbach, L.H. Caporales, J.J. Levy, R.F. Nutt, M. Rosenblatt, D.C. Tosteson, Primary structure of peptides and ion channels, Biophys. J. 58 (1990) 1367–1375.
[42] M.T. Tosteson, D.C. Tosteson, The sting. Melittin forms channels in lipid bilayers, Biophys. J. 36 (1981) 109–116.
[43] H. Vogel, F. Jähnig, The structure of melittin in membranes, Biophys. J. 50 (1986) 573–582.
[44] J.E. Hall, I. Vodyanoy, T.M. Balasubramanian, R. Marshall, Alamethicin. A rich model for channel behavior, Biophys. J. 45 (1984) 233–247.
[45] J.C. Phillips, R. Braun, W. Wang, J. Gumbart, E. Tajkhorshid, E. Villa, C. Chipot, R.D. Skeel, L. Kale, K. Schulten, Scalable molecular dynamics with NAMD, J. Comput. Chem. 26 (2005) 1781–1802.
[46] W. Humphrey, A. Dalke, K. Schulten, VMD — visual molecular dynamics, J. Mol. Graph. 14 (1996) 33–38.
[47] M. Bachar, O.M. Becker, Melittin at a membrane/water interface: effects on water orientation and water penetration, J. Chem. Phys. 111 (1999) 8672–8685.
[48] M. Manna, C. Mukhopadhyay, Cause and effect of melittin-induced pore formation: a computational approach, Langmuir 25 (2009) 12235–12242.
[49] S.E. Blondelle, R.A. Houghten, Hemolytic and antimicrobial activities of the twenty-four individual omission analogues of melittin, Biochemistry 30 (1991) 4671–4678.
[50] M. Mihajlovic, T. Lazaridis, Antimicrobial peptides bind more strongly to membrane pores, Biochim. Biophys. Acta 1798 (2010) 1494–1502.
[51] B. Bechinger, Structure and functions of channel-forming peptides: magainins, cecropins, melittin and alamethicin, J. Membr. Biol. 156 (1997) 197–211.
[52] S.V. Rudenko, E.E. Nipot, Protection by chlorpromazine, albumin and bivalent cations against haemolysis induced by melittin, [Ala-14]melittin and whole bee venom, Biochem. J. 317 (1996) 747–754.
[53] S. Rex, A Pro→Ala substitution in melittin affects self-association, membrane binding and pore-formation kinetics due to changes in structural and electrostatic properties, Biophys. Chem. 85 (2000) 209–228.
[54] C.E. Dempsey, R. Bazzo, T.S. Harvey, I. Syperek, G. Boheim, I.D. Campbell, Contribution of proline-14 to the structure and actions of melittin, FEBS Lett. 281 (1991) 240–244.
[55] A. Zemel, D.R. Fattal, A. Ben-Shaul, Energetics and self-assembly of amphiphatic peptide pores in lipid membranes, Biophys. J. 84 (2003) 2242–2255.
[56] D.N. Woolfson, R.J. Mortishire-Smith, D.H. Williams, Conserved positioning of proline residues in membrane-spanning helices of ion-channel proteins, Biochem. Biophys. Res. Commun. 175 (1991) 733–737.
[57] K.A. Williams, C.M. Deber, Proline residues in transmembrane helices: structural or dynamic role? Biochemistry 30 (1991) 8919–8923.
[58] R.B. Best, N.-V. Buchete, G. Hummer, Are current molecular dynamics force fields too helical? Biophys. J. 95 (2008) L07–L09.
[59] K. Hall, T.-H. Lee, M.-I. Aguilar, The role of electrostatic interactions in the membrane binding of melittin, J. Mol. Recognit. 24 (2011) 108–118.
[60] N. Asthana, S.P. Yadav, J.K. Ghosh, Dissection of antibacterial and toxic activity of melittin. A leucine zipper motif plays a crucial role in determining its hemolytic acitivity but not antibacterial activity, J. Biol. Chem. 279 (2004) 55042–55050.
[61] E.S. Salnikov, H. Friedrich, X. Li, P. Bertani, S. Reissmann, C. Hertweck, J.D.J. O'Neil, J. Raap, B. Bechinger, Structure and alignment of the membrane-associated peptaibols ampullosporin A and alamethicin by oriented ^{15}N and ^{31}P solid-state NMR spectroscopy, Biophys. J. 96 (2009) 86–100.